Research Square

Preprints are preliminary reports that have not undergone peer review.
They should not be considered conclusive, used to inform clinical practice,
or referenced by the media as validated information.

Concentration-Dependent Electronic and Optical Properties of Cr-Doped α-Al_2O_3: A First-Principles DFT Study

Taha Yasin Ahmed

taha.ahmed@univsul.edu.iq

University of Sulaimani

Shujahadeen B. Aziz

University of Sulaimani

Research Article

Keywords: α-Al_2O_3 metal oxide, DFT&GGA approximation, Band structure & PDOS study, optoelectronic properties, Absorption edge and Tauc model

Posted Date: November 3rd, 2026

DOI: https://doi.org/10.21203/rs.3.rs-11405556/v1

License: This work is licensed under a Creative Commons Attribution 4.0 International License.
Read Full License

Additional Declarations: No competing interests reported.

Concentration-Dependent Electronic and Optical Properties of Cr-Doped α-Al_2O_3: A First-Principles DFT Study

Taha Yasin Ahmed[1*], Shujahadeen B. Aziz [2,3]

[1] Physics Department, College of Science, University of Sulaimani, Qlyasan Street, Sulaimaniyah 46001, Iraq.
[2]Research and Development Center, University of Sulaimani, Qlyasan Street, Kurdistan Regional Government, Sulaymaniyah 46001, Iraq.
* Corresponding author email: taha.ahmed@univsul.edu.iq

Abstract

Chromium (Cr) substitution offers a route to modifying the electronic structure and optical response of α-Al_2O_3, a wide-band-gap oxide with limited intrinsic absorption in the visible region. In this study, the concentration-dependent electronic and optical properties of Cr-doped α-Al_2O_3 are investigated using spin-polarized density functional theory within the generalized gradient approximation of Perdew–Burke–Ernzerhof, as implemented in VASP. Substitutional Cr concentrations of 8.33% and 16.66% are considered. The electronic structure is examined through band-structure and total and partial density-of-states analyses, while the optical response is evaluated using the complex dielectric function, energy-loss function, refractive index, extinction coefficient, absorption coefficient, and Tauc analysis. The calculated band gap decreases from 6.47 eV in pristine α-Al_2O_3 to 1.75 eV and 0.57 eV at Cr concentrations of 8.33% and 16.66%, respectively. The electronic-structure analysis indicates the formation of Cr-derived states within the host band gap, providing a qualitative explanation for the concentration-dependent gap narrowing and the shift of optical absorption toward lower photon energies. The optical results further demonstrate that Cr substitution substantially modifies the calculated light-response characteristics of α-Al_2O_3. These findings highlight the potential of substitutional doping as a means of tuning the electronic and optical properties of alumina. However, the absolute band-gap values should be interpreted cautiously because of the known limitations of the PBE functional and the relatively high dopant concentrations represented by the periodic models.

Key words: α-Al_2O_3 metal oxide; DFT&GGA approximation; Band structure & PDOS study; optoelectronic properties; Absorption edge and Tauc model.

1. Introduction

Aluminum oxide (Al_2O_3) is widely recognized as an important material for ceramic, optical, and electronic applications owing to its excellent thermal stability, chemical resistance, and mechanical hardness. Among its different crystalline phases, α-alumina (α-Al_2O_3) is the most thermodynamically stable polymorph and crystallizes in the hexagonal corundum structure. These

characteristics have made α-Al_2O_3 suitable for various applications, including optical coatings, optoelectronic components, electroluminescent displays, transparent ceramics, and laser-host materials [1,2,5]. Its dielectric characteristics and low leakage current have also attracted interest in electronic devices, particularly metal–oxide–semiconductor (MOS) gates and charge-trapping memory systems [3]. Other alumina polymorphs, such as β-, γ-, δ-, θ-, and κ-Al_2O_3, have also been investigated; however, many metastable phases tend to transform into the stable α-phase during high-temperature treatment [4]. In addition, alumina nanoparticles and alumina-based materials have been explored for adsorption and catalytic applications because of their useful physicochemical and surface properties [6].

Despite these advantages, the large band gap of α-Al_2O_3 is a major limitation for applications requiring efficient absorption of visible light. Reported band-gap values depend on the experimental technique, computational approach, and alumina phase under investigation [7–11]. Previous studies have employed different theoretical and experimental methods to estimate the electronic gap of alumina, reporting values that vary considerably across the literature. For example, Samantaray et al. investigated γ-Al_2O_3 using the local-density approximation (LDA), whereas other studies used UV–visible spectroscopy, generalized gradient approximation (GGA) calculations, and the full-potential linearized augmented plane-wave (FP-LAPW) method to evaluate its electronic or optical properties [7–11]. The wide band gap of α-Al_2O_3 means that its intrinsic optical response is concentrated mainly in the ultraviolet region, limiting its direct utilization of visible-light photons. One strategy for addressing this limitation is chemical doping, which can modify the electronic structure through the introduction of dopant-derived states within the host band gap. Depending on the dopant and its concentration, these states may reduce the calculated band gap and shift the optical absorption edge toward lower photon energies [12].

Transition-metal doping is particularly relevant because the partially occupied d orbitals of these elements can interact with the electronic states of the host material. Chromium (Cr) is an interesting dopant for α-Al_2O_3 because Cr-related electronic states can influence its band structure and optical response. Furthermore, Cr^{3+}-doped α-Al_2O_3 is well known for its characteristic optical emission and its use in laser materials, demonstrating the importance of chromium in alumina-based optical systems [13]. Separately, alumina-containing composites have been investigated for catalytic processes, including the degradation of organic pollutants, where surface adsorption and other material characteristics can contribute to performance [14]. Nevertheless, changes in the band gap or absorption spectrum alone are insufficient to establish the suitability of a doped material for a particular photocatalytic or photovoltaic application.

Density functional theory (DFT) has become a widely used approach for examining the atomic-scale structural, electronic, and optical characteristics of functional materials. Previous first-principles investigations have applied DFT to oxides, hydrides, perovskites, and other semiconducting systems to explore their electronic structures and optical responses [15–19]. For alumina-based materials, DFT calculations can provide insight into the influence of chemical substitution on the band structure and the distribution of electronic states. In particular, band-structure calculations and total and partial density-of-states (TDOS and PDOS) analyses can help identify the contributions of dopant orbitals to the electronic states near the valence- and conduction-band edges [20–29]. Optical calculations based on the complex dielectric function can complement these analyses by providing information about the dielectric response, refractive index, extinction coefficient, absorption coefficient, and energy-loss function. Examining these properties together offers a more comprehensive theoretical description of how dopant concentration affects the electronic and optical behavior of a material. However, direct assessment

of photocatalytic or photovoltaic performance also requires additional information, such as band-edge alignment, charge-carrier recombination, and charge transport, which cannot be established solely from band-gap and optical-spectrum calculations.

In the present work, first-principles DFT calculations implemented in the Vienna *Ab initio* Simulation Package (VASP) are employed to investigate the concentration-dependent electronic and optical properties of Cr-doped α-Al_2O_3. Chromium substitutes for aluminum at two concentrations, namely 8.33% and 16.66%, allowing the effects of increasing Cr content to be compared within the adopted computational models. The electronic properties are examined using band structures and TDOS and PDOS analyses. The optical response is investigated through the complex dielectric function and its derived optical constants, including the refractive index, extinction coefficient, and absorption coefficient. The energy-loss function and Tauc analysis are also considered to provide complementary perspectives on the calculated optical response. Particular emphasis is placed on the evolution of the band gap, the contribution of Cr-related electronic states, and the relationship between changes in the electronic structure and the resulting optical characteristics.

The principal objective of this study is to establish a comparative theoretical description of how Cr concentration influences the electronic and optical properties of α-Al_2O_3. By combining band-structure and density-of-states analyses with several optical-response functions, the work examines the relationship between dopant-induced electronic states, band-gap modification, and changes in optical absorption. This integrated analysis provides a basis for understanding the optical-response engineering of Cr-doped alumina and for identifying questions that may be addressed in subsequent experimental and theoretical investigations. The calculated results should be interpreted with consideration of the limitations of the PBE exchange–correlation functional,

particularly its tendency to underestimate band gaps, as well as the relatively high dopant concentrations represented by the periodic models. Accordingly, the findings describe the predicted electronic and optical properties of the investigated systems and do not, by themselves, demonstrate improved photovoltaic efficiency or photocatalytic activity.

2. Computational Detail

The Vienna Ab initio Simulation Package (VASP) was used to perform the first-principles calculations within the plane-wave pseudopotential framework [30]. The exchange correlation potential was calculated using the GGA method and the Perdew-Burke-Ernzerhof functional approach. The optical, density of states, band structure, and geometry optimization were calculated using this functional technique [31]. The unit cell of α-Al_2O_3, which contains 30 atoms in the conventional hexagonal unit cell, a space group of R3c, 18 four-coordinated O atoms, and 12 six-coordinated Al atoms, is shown in Figure 1(a). Additionally, a substitutional model was used as demonstrated in Figures 1(b) and 1(c). The substitution of Cr atoms in the Al sites was achieved at the octahedrally coordinated sites in the α-Al_2O_3 structure. Other non-equivalent Al sites were also studied in preliminary calculations to obtain qualitatively similar electronic and optical properties, hence confirming the selected substitutional site. The substitution of Cr was done by replacing either one or two of the Al atoms with Cr atoms in the Al sites of the α-Al_2O_3 structure. The adopted supercell has a substitution of one Al atom by one Cr atom giving rise to $Al_{11}CrO_{18}$ structure with a substitutional concentration of Cr atoms at 8.33%, while substitution of two Al atoms by two Cr atoms gives rise to the composition $Al_{10}Cr_2O_{18}$, with a substitutional concentration of Cr atoms at 16.66%.

In addition, regarding the spin contributions, it is worth mentioning that chromium is a magnetic material; thus, spin-polarized calculations are used in this study. In fact, the magnetic moment value is approximately 3.87 μ_B, which shows that the spin contributions are significant in the Cr-doped material. It is worth mentioning that chromium is a transition metal that has unpaired d-electrons; thus, it has the ability to contribute magnetism that may affect the band gap value. Therefore, spin-polarized density functional theory calculations are essential for correctly evaluating the magnetic contributions on the band gap value of the Cr-doped α-Al_2O_3 material. For both the pristine and Cr-doped α-Al_2O_3 systems, a plane-wave energy cutoff of 380 eV and a Monkhorst-Pack k-point mesh of 15x15x4 were used for Brillouin-zone sampling [32-34]. The electronic self-consistent field (SCF) calculations were assumed to be converged when the difference of the total energy between two consecutive electronic steps was less than 1.0×10 -4 eV. For ionic relaxation calculations, the force convergence criterion was set to 1.0 × 10 −2 eV/Å. The maximum atomic force was 0.005417 eV/Å for the pristine α-Al_2O_3 system and 0.0078 eV/Å for the doped systems. In addition, the calculated total energies were −249.52958476 eV, −286.02521519 eV, and −254.47322326 eV for pristine α-Al_2O_3 and Cr-doped α-Al_2O_3 with 8.33% and 16.66% Cr concentrations, respectively. It is pertinent to mention here that phonon calculations were not performed in the present study; therefore, the dynamical stability of the optimized structures doped with chromium was not investigated through phonon calculations in this study, thus no determination of dynamical stability could be achieved. The calculated properties are properties of the optimized structures under the employed DFT calculation. A determination of dynamical stability can only be achieved via phonon dispersion or phonon density of states calculations where the absence of imaginary frequencies proves dynamical stability. The calculated structural and electronic properties should consequently be interpreted as properties of the

optimized configurations, while a definitive assessment of dynamical stability requires phonon dispersion or phonon density-of-states calculations.

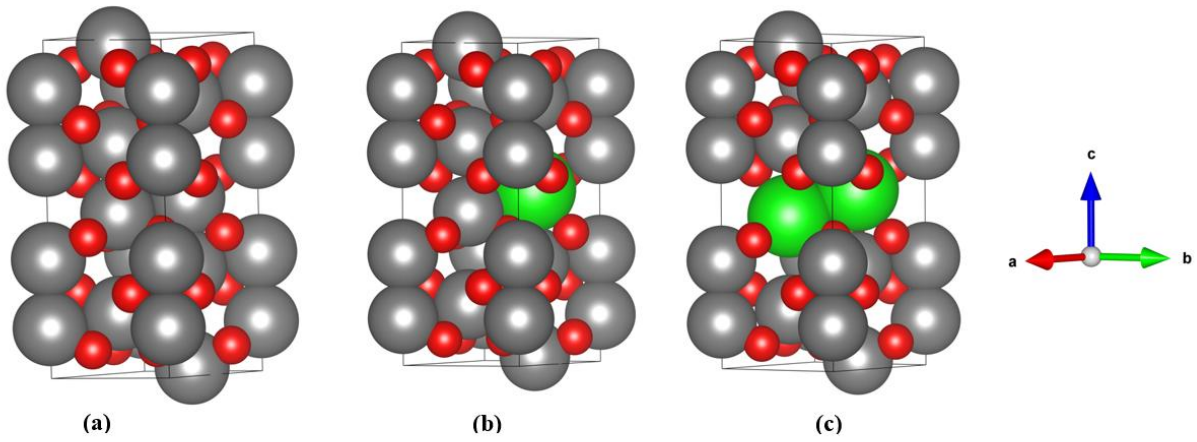


Figure 1: Crystal structures of (a) pristine α-Al_2O_3, (b) 8.33% substitutional Cr-doped α-Al_2O_3 ($Al_{11}CrO_{18}$), and (c) 16.66% substitutional Cr-doped α-Al_2O_3 ($Al_{10}Cr_2O_{18}$).

3. Result and Discussion

3.1 Structural optimization and formation energy

The GGA approach with PBE exchange-correlation functional utilized in this study yielded optimal lattice parameters of $a = b = 4.76$ Å, $c = 12.99$ Å [6], which are quite similar to the experimental lattice parameters of $a = b = 4.7563$ Å, $c = 12.9820$ Å [35]. It is important to note that there is relatively little variation between the calculated and observed lattice parameters. Table 1 presents the optimized lattice parameters for both pure and Cr-doped α-Al_2O_3 after structural relaxation. The calculated lattice parameters for pure Al_2O_3 was found consistent well with prior theoretical results. The increase in Cr concentration results in a minor reduction in the

a parameter and a rise in the c parameter. This implies that anisotropic lattice distortion is caused by the Cr substitution. The slight variations in the lattice parameters and volume of the optimized unit cell suggest that the chromium-doped systems are capable of being relaxed without any significant change in the total α-Al_2O_3 structure. Nevertheless, structural properties alone cannot define mechanical and dynamical stability.

Table 1. Structural parameters of pure and Cr-doped α-Al_2O_3 after geometry optimization.

Structure	**Description**	$a = b$ (Å)	c (Å)	V (Å^3)	$\alpha = \beta$ (°)	γ (°)	**Formation energy (eV)**
Al_2O_3	Pure	4.76	12.99	249.97	90	120	0
Cr: α-Al_2O_3 (8.33%)	$Al_{11}CrO_{18}$	4.7475	13.03	251.70	90	120	-1.375
Cr: α-Al_2O_3 (16.66%)	$Al_{10}Cr_2O_{18}$	4.70	13.1375	252.52	90	120	-2.245

From the obtained results in this study, it can be concluded that lattice parameters a and c obtained in this study fall into the range of lattice parameters obtained in other studies, namely lattice parameters $a = 4.74 - 4.82$ Å, $c = 12.94 - 13.16$ Å. Naturally, some differences exist between the obtained results in this study and other studies, since different exchange-correlation functionals and computational methods, namely the LDA method, GGA method, FP-LAPW method, HSE method, etc., are used [10, 11, 36, 37, 38]. It is found that the optimized structure is

suitable for the investigation of the doped α-Al_2O_3 systems, and a good agreement could be seen between the calculated results of the current study and those reported previously.

The chemical stability of the pure and chromium doped α-Al_2O_3 has been analyzed in the present study by employing the formation energy concept to validate the stability of the created supercell systems. There exist multiple studies that have either failed to incorporate the stability of the system by using formation energy or phonon calculation techniques [10, 11,36], or else have emphasized mechanical stability [39-41], or adopted phonon dispersion approach to prove their dynamic stability [42]. Formation energy and phonon methodologies are thus extensively utilized in the density functional theory approach. As one can notice from Table 1, the analysis of the results is not hard to conduct based on the formalism of the defect formation theory. The latter provides the formation energy formula which includes the difference in energies of two systems and chemical potentials of elements forming the aforementioned two systems. In this specific case, it is necessary to suppose that doping of α-Al_2O_3 with Cr is associated with the addition of Cr atoms and removal of Al atoms with an aim of charge compensation. Therefore, there is addition of Cr atoms controlled by μCr and removal of Al atoms controlled by μAl. Since the initial energy of pure α-Al_2O_3 equals zero eV, one can deduce that negative values of the formation energy (−1.375 eV and −2.25 eV) point to thermodynamic feasibility of the process. Moreover, reduction of the negative values means that doping with Cr atoms becomes more energetically favorable. It should also be noted that the constant values of μAl and μCr mean that the presented data was obtained under identical growth conditions. The calculated formation energies indicate that Cr substitution is energetically favorable under the selected chemical-potential conditions; however, these results alone cannot establish the overall stability of the Cr-doped systems. Mechanical stability requires the calculation of elastic constants, whereas dynamical stability requires phonon calculations.

Since these calculations were not performed in the present study, no definitive conclusions can be drawn regarding the mechanical and dynamical stability of the Cr-doped systems. Future work will therefore include a detailed investigation of dynamical stability through phonon density-of-states and phonon-dispersion calculations. Such calculations would also provide further insight into the role of electron–phonon interactions in properties such as carrier lifetimes, optical absorption, and luminescence.

3.2 Calculated Band Gap Study

3.2.1 Band structure

The electronic band structure and density of states provide important information about the electronic properties and band-gap characteristics of a material. A material's electronic band structure can determine the possibilities of the energy ranges occupied by the free electrons, known as the energy bands. The band gap, as indicated by the orange arrow in Figure 2, is the range between the valence band maximum (VBM) and the conduction band minimum (CBM) where no electronic states are available in the ideal band structure [43]. Therefore, the band gap relates to the ranges of energy where the free electrons are not allowed. The energy required to move a valence electron associated with an atom to a conduction electron while creating a hole in the valence band (VB) is termed the band gap energy, E_g. In the crystal lattice, the created hole and the promoted conduction electron are free to move and are responsible for the conduction of an electric current. Materials may be classified as conductors, semiconductors, or insulators depending on their band gaps. Materials with sufficiently large band gaps exhibit insulating behavior, whereas smaller band gaps generally correspond to semiconducting behavior [44].

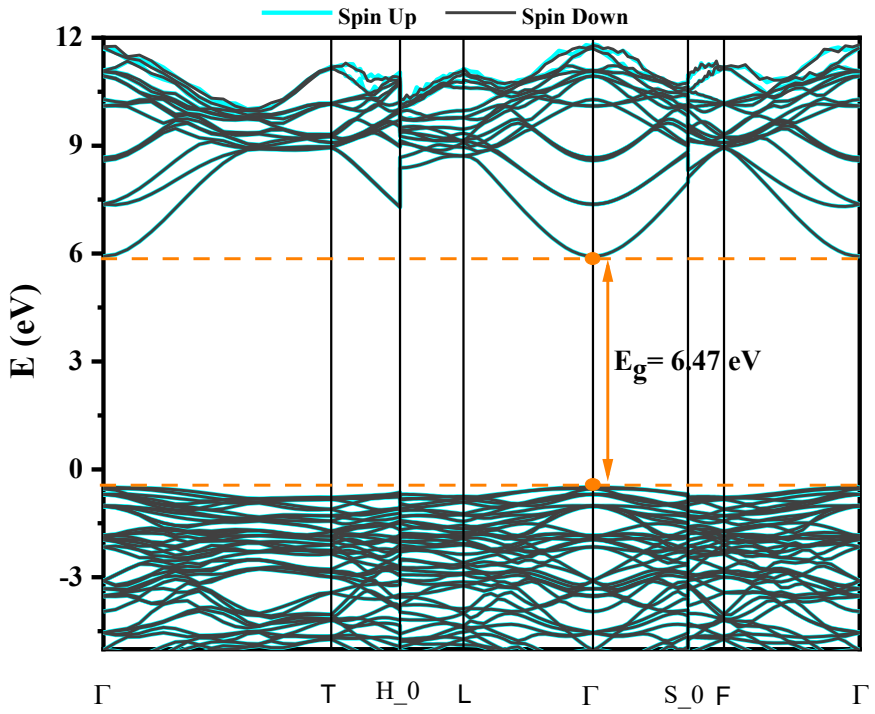


Figure 2: Calculated band structure of pure α-Al_2O_3.

Figure 2 shows a high-symmetry path in the Brillouin zone (Γ-T-H-0-L-Γ-S-0-F-Γ) that represents the band structure of the virgin system. In contrast, the band structures of Cr-doped Al_2O_3 are shown in Figures 3 and 4 along a high-symmetry path in the Brillouin zone (Γ-M-K-Γ-A-L-H) for doping samples. Both the valence band maximum and the conduction band minimum are located in a high-symmetry site, as shown by the orange dashed line in Figure 2. The atomic number of aluminum is 13, and its electronic configuration is [Ne] $3s^2$ $3p^1$. Conversely, oxygen has an electrical configuration of $1s^2$ $2s^2$ $2p^2$ with an atomic number of 8. While nonbonding O-p states dominate the upper valence bands, contributions from Al-3s states cause a broad minimum for the

conduction band at the Γ-point. This is in line with most of the previous studies that have shown that alumina has a direct band gap [10, 37]. The calculated band gap, shown in Figure 2, is 6.47 eV, which is in agreement with earlier study [30]. To investigate the role of the main and impurity energy levels, we calculated the band structure, as presented in Figures 3 and 4. The calculated band gap clearly indicates that the band gap decreases with an increase in dopant concentration. For instance, the band gap is decreased from 6.47 eV for the pure system to 1.75 eV and 0.57 eV for 8.33% Cr and 16.66% Cr concentrations, respectively. This is due to the properties of the dopant, as it is known that the atomic number of Cr is 24 with an electronic configuration of [Ar] $3d^5 4s^1$. This adds impurity levels in the band gap but does not affect the valence band. With increased dopant concentration, more free electrons are available in the donor states in the band gap. In addition, it is important to mention that It should be highlighted that the calculated band-gap values, especially the very small value of 0.57 eV for the 16.66% Cr doped α-Al_2O_3 system, should not be regarded as quantitatively accurate predictions of the experimental band gap. Instead these values should be viewed mainly as a measure of systematic tendency of Cr-induced band-gap narrowing. The relatively high concentration of Cr in the periodic supercell can promote the interaction between the periodically repeated Cr atoms and facilitate the formation of impurity bands. It is well known that the GGA-PBE exchange-correlation functional tends to underestimate the absolute band gaps of semiconductors and insulators. The present calculations should be more reliable in describing the qualitative evolution of the electronic structure, such as the formation of Cr-induced impurity states and the progressive narrowing of the band gap, than predicting its absolute magnitude. To obtain more accurate quantitative values for the band-gap, more sophisticated approaches are required, such as hybrid functionals or many-body methods.

In Cr-doped Al_2O_3 at a concentration of 8.33%, it is observed that the transition is indirect, with VBM at the Γ-point and CBM at the K-point, as shown in Figure 3. However, in the case of 16.66% Cr concentration, it is observed that the transition is direct, as shown by the dashed line in Figure 4 and near the high-symmetry Γ-point. As it can be seen in Figure 3, for Cr-doped alumina (α-Al_2O_3) with 8.33 wt.%, the change in electronic band structure is clear in the presence of a transition metal and obvious that a large bandgap insulating material could be transferred into a semiconductor. Figure 3 and the discussion is connected to the spin-polarized system and electronic properties. Figure 3, illustrates that there are different electronic states for the Spin-Up (cyan) and Spin-Down (red) channels. The large difference between the two channels, in particular for the Fermi level (E=0 eV), determines the strong magnetic moment present in the Cr-doped alumina. This is a common effect in dilute magnetic semiconductors or insulators and is due to the 3d orbitals of the transition metal forming new states within the original bandgap [45].

The bandgap (E_g) is clearly identified as 0.57 eV. The presence of orange dots at the Γ-point indicates that it is a direct bandgap. This is a significant reduction in comparison to pure alumina, where the wide bandgap is ~8.8 eV [46]. Mid-gap States are also clearly identified. The presence of narrow bands between -1 eV and 1 eV is due to the presence of Cr-3d states. These states are split due to the crystal field of the alumina lattice, effectively "closing" the wide gap of the host and turning it into a narrow-gap material [47]. However, it is important to mention here that caution is required while interpreting the substantial reduction in the band gap energy with the increase in the Cr contents. Despite the presence of the evidence showing the formation of impurity electronic states with increasing trends in the band gap reduction with increasing doping levels, there can be certain limitations in the absolute values obtained for such high doping levels as the calculation method is prone to errors due to high doping levels and the use of periodic supercell approximation

technique in the calculations. Thus, under the effect of these factors, enhanced interactions among Cr atoms inside the simulation box can lead to impurity-band formation and substantially modify the semiconducting character of the system. The present work is focused mainly on providing information about changes in the properties of the system due to Cr incorporation.

In addition, our study uses the GGA-PBE functional, the performance of which has been noted to be generally underestimate band gaps because of the basic treatment of exchange-correlation. This means that the band gap 6.47 eV for α-Al_2O_3 is smaller than the true band gap of 8.8 eV. The band gaps can be better predicted using hybrid functional methods such as the HSE06 functional, but these methods are very time-consuming, especially for large supercell systems in the doping process [48-52]. While this might be a limitation, however, the application of PBE is reasonable because the aim of this research work is not to accurately reproduce the band gap measured experimentally but rather to determine qualitative changes brought about by doping. Some of these qualitative changes include the narrowing of band gap, formation of states due to impurities, and changes in optical absorption due to doping.

The x-axis indicates that the path of the Brillouin zone is $\Gamma \rightarrow M \rightarrow K \rightarrow \Gamma \rightarrow A \rightarrow L \rightarrow H$. The level of dispersion, or how curvy the lines are, is relatively flat for the Cr-induced states at the Fermi level, indicating high levels of localization for the electrons, which is typical in d-electron systems [53].

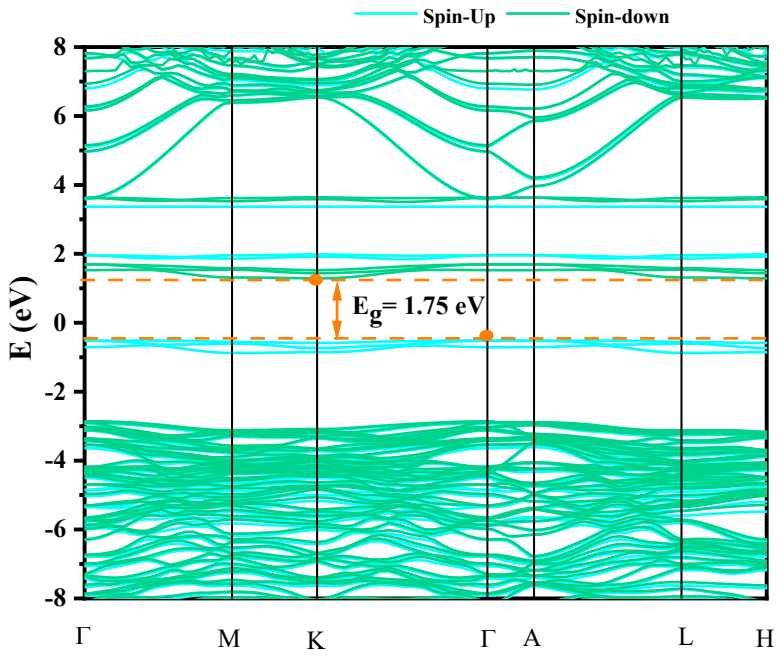


Figure 3: Calculated band structure of 8.33% substitutional Cr-doped α-Al_2O_3.

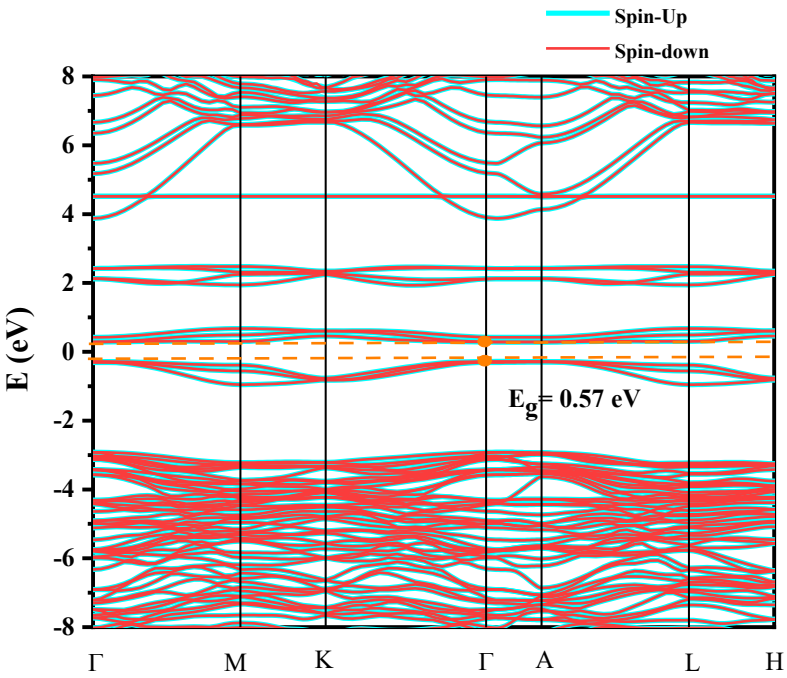


Figure 4: Calculated band structure of 16.66% substitutional Cr-doped α-Al_2O_3.

To better place the present work in the frame of previous first-principles investigations, comparison with representative DFT studies on doped α-Al_2O_3 is summarized in Table 2. It has been shown that substitutional doping is a successful route for the modification of the electronic structure and the optoelectronic properties of α-$Al_2 O_3$. However, the degree of band-gap reduction is strongly dependent on the dopant species, dopant concentration and the electronic interaction between the dopant orbitals and the host lattice. For the p-block dopants, Tl-doped α-Al_2O_3 exhibits considerable changes in its electronic structure, according to the report by Ahmed et al. [6] the band gap shrinks from 6.47 eV at an initial value to 3.15 and 2.38 eV at concentrations of 8.33% and 16.66% of Tl atoms, respectively. Such behavior was explained by the appearance of impurity states associated with the presence of Tl ions, leading to a red shift in the absorption edge, as well as enhanced dielectricity, increased refractive index, and higher optical conductivity. This effect was also found in α-Al_2O_3 doped with In-, B-, and As-atoms, having their band gaps decreased to 4.91, 4.25, and 3.25 eV, respectively. It should be noted that As was the most efficient in reducing the band gap among other elements considered [54]. Similar behavior has also been observed in the case of dopants from group IIIB. Benam et al. [55] studied the effect of Sc, Y, La, and Ac dopants on the electronic structure of α-Al_2O_3 with substitution of 25% and concluded that all dopants decrease the band gap compared to pure α-Al_2O_3. Nevertheless, the effect of reduction is different for different dopants. The band gaps obtained with Sc and Y dopants are smaller and amount to 6.52 and 6.07 eV, respectively, while in the case of La and Ac the reduction of band gap is significantly larger, and it amounts to 2.91 and 2.39 eV, respectively. This can be attributed to the growth of ionic radii of dopants and their increased interaction with the states of host crystal. The doping of transition metal has been observed to give a more pronounced effect on the

electronic structure due to partial occupation of the d orbitals. It was revealed by Rahnamaye Aliabad et al. [56] that the incorporation of Co into α-Al_2O_3 at about 8.35 at.% forms Co-3d orbitals which have strong interactions with O-2p orbitals and consequently reduce the energy gap to about 2.0 eV, while at the same time increasing the optical activity of α-Al_2O_3. Similarly, the experiments carried out by Hamdan et al. [57] regarding doping of α-Al_2O_3 with Cr have demonstrated that Cr incorporation reduces the energy gap from 6.70 to 2.45 eV and increases its optical activity.

In comparison with previous theoretical works described in Table 2, the current study suggests an even stronger modification of the electronic structure. Substituting Cr in the amount of 8.33% and 16.66% results in a remarkable reduction of the calculated band gap from 6.47 eV for the pristine α-Al_2O_3 to 1.75 and 0.57 eV respectively. These numbers, and in particular the 0.57 eV at 16.66% Cr concentration, should be taken with caution, because of the known limitations of the GGA-PBE functional and the periodic supercell representation at relatively high dopant concentration. The main implication of these results is the systematic trend of Cr-induced band-gap narrowing and the increasing contribution of Cr-3d impurity states to the electronic structure. An increase of the Cr concentration is accompanied by an increase of the role of these impurity states, leading to more intense band-gap narrowing and optical absorption in the visible range with an increase of dielectric constant. These results are in full accordance with the general mechanism of the electronic structure modification, suggested in the previous first-principles calculations – substitutional doping creates dopant-related impurity states and, thus, leads to changes in the electronic structure. It should be noted, however, that the effect of Cr on α-Al_2O_3 is especially strong in comparison with other dopants studied earlier.

Table 2. Comparison of reported band-gap engineering in doped α-Al_2O_3 from first-principles studies and the present work.

Material/System	Dopant concentration (%)	Pure Band Gap (eV)	Calculated band gap (eV)	Reference
Tl-doped α-Al_2O_3	8.33 16.66	6.47	3.15 2.38	6
In-doped α-Al_2O_3	8.33	6.47	4.91	54
B-doped α-Al_2O_3	8.33	6.47	4.25	
As-doped α-Al_2O_3	8.33	6.47	3.25	
Sc-doped α-Al_2O_3	25	6.57	6.52	55
Y-doped α-Al_2O_3	25	6.57	6.07	
La-doped α-Al_2O_3	25	6.57	2.91	
Ac-doped α-Al_2O_3	25	6.57	2.39	
Co-doped α-Al_2O_3	8.35	6.3	2	56
Cr-doped α-Al_2O_3	0.8 wt%	6.70	2.45	57
Cr-doped α-Al_2O_3	8.33 16.66	6.47	1.75 0.57	Present work

To get an insight of the contribution of individual atomic orbitals in the electronic structure of pure and Cr doped α-Al_2O_3, TDOS and PDOS calculations have been done, as shown in Figure 5-7. These calculations provide a detailed insight into the electronic states and the influence of the dopant elements. For a system in which the electrons are in a paired state, TDOS and PDOS are usually symmetric for a given direction of the spin. But, in the presence of dopant elements, there may be some unpaired electrons and, in such cases, the DOS may be unsymmetric. Such changes may result in the development of magnetic moments. But in the present work, we focus on the

modification in the electronic structure and band gap. Figure 5 displays the TDOS and PDOS of pristine α-Al_2O_3. It is found that the VB is mainly composed of O-2p states and ranges from -10 to 0 eV. In addition, the CB is mainly composed of Al-3s states with partial hybridization with O-2p states, ranging from 6.75 to 12 eV. In general, the VB is mainly composed of O-2p states, while the CB is mainly composed of metal s-states, as mentioned in the previous studies that the valence band of most metal oxides is mainly composed of O-2p orbitals, while the metal s states mainly compose the conduction band [58]. In addition, the energy range from 0 to 6.47 eV is the band gap of the pristine α-Al_2O_3.

Figures 6 and 7 present the TDOS and PDOS of Cr doped α-Al_2O_3 at concentrations 8.33% and 16.66%, respectively. Two regions of the VB are present in the system of Cr doped α-Al_2O_3 at 8.33% concentration (Figure 6). The first region, located between -10 and -2 eV, consists of O-2p orbitals and a smaller contribution of Al-3s orbitals. The second region, located between -2 and 0 eV, includes a strong peak of Cr-3d orbitals. These orbitals indicate the presence of impurity states, having a much stronger intensity than the O-2p orbitals. In addition, the CB is affected by the existence of Cr-3d states: Because of the impurity states, there are two zones in the conduction band. The higher conduction band spans from 3.5 to 10 eV, while the lower conduction band spans from 1.75 to 2.5 eV. The influence of Cr-3d states around the Fermi level increases for both spin-up and spin-down channels when the concentration of Cr rises to 16.66%, as seen in Figure 7. This narrows the band gap even more. The TDOS and PDOS analysis clearly demonstrate the introduction of intermediate electronic states in the energy region of the forbidden energy gap of the α-Al_2O_3 crystal lattice by Cr doping. While pure alumina is a well-known wide band-gap insulator (with a band-gap energy of 8.8 eV) [41], the Cr-3d states lead to the formation of impurity states within the band-gap. These intermediate states, mainly located between -1 and 3 eV,

influence the electronic properties of the material, turning it into a semiconductor, depending on the dopant concentration [59]. To better understand the origin of this band structure, a PDOS was examined. Below the Fermi level, the valence band (between -10 and -3 eV) is composed mainly of O-2p orbitals hybridised with Al-3s and a small fraction of Cr-3d orbitals, due to the partial covalent character of the Al-O and Cr-O bonds [60]. On the other hand, the conduction band (6 eV to 10 eV) is a combination of Al, O and Cr orbitals. The octahedral coordination of the Al site in α-Al_2O_3 results in crystal-field splitting of the Cr-3d orbitals into t_2g (lower energy) and e_g (higher energy) orbitals, enabling the formation of the impurity states observed in the DOS [61].

In addition to this, the spin-resolved TDOS and PDOS have revealed the magnetic properties of α-Al_2O_3 doped with Cr. The asymmetry between the spin-up and spin-down Cr-3d contributions indicates spin polarization and is consistent with the calculated magnetic moment of approximately 3.87 μB per Cr atom. It is evident from the above discussion that doping with Cr not only changes the electronic properties of α-Al_2O_3 by introducing impurities in the gap state, but it also gives rise to magnetic properties [62]. The origin of the Cr-induced change of the electronic, magnetic and optical properties can be understood by means of the calculated band structures and spin-resolved DOS/PDOS. The substitution of Al by Cr introduces partially filled and spin-polarized Cr-3d states into the electronic structure of a-Al2O3. These Cr-3d states interact with the neighboring O-2p orbitals leading to a Cr-3d/O-2p hybridization and the formation of extra Cr-derived electronic states near the band edges. Therefore, the electronic structure is strongly modified, giving rise to a progressive reduction of the calculated band gap from 6.47 eV for pristine a-Al2O3 to 1.75 eV and 0.57 eV for the studied Cr concentrations. The spin polarization of the partially filled Cr-3d states is also responsible for the calculated magnetic moment of about 3.87 muB per Cr atom. Introduces additional low-energy electronic states that can contribute to lower-energy optical

transitions, which results in a shift of the absorption edge toward lower photon energies and an enhancement of the optical response in the Cr-doped systems. Recent computational studies on semiconductor and optoelectronic materials have reported similar correlations between electronic-structure modification and optical behavior [63,64]. Thus, the derived DOS/PDOS, magnetic moment, band-gap reduction, and optical spectra suggest that the Cr incorporation significantly alters the electronic structure of α-Al 2 O 3 through the spin-polarized Cr-3d states and their coupling with the neighboring O-2p states.

Physical connection between electronic and optical properties: The modification of the optical properties caused by Cr substitution can be directly linked to the modifications of the electronic structure. For pure α-Al_2O_3, the valence band region is formed predominantly of O-2p states, whereas the conduction band region has contributions from the Al-related states, giving rise to a large band gap. On Cr substitution for Al, partially filled and spin-polarized Cr-3d states are introduced in the forbidden energy region. These Cr-3d states hybridize with O-2p orbitals to create Cr-3d/O-2p impurity states inside the band gap of the host. As the concentration of the dopant increases, the role of these states grows, and the energy difference between the occupied and unoccupied states decreases. Consequently, the decrease of the band gap makes it possible to achieve optical transitions using lower energy photons; hence, the absorption edge is shifted into the visible and infrared region of the spectrum. Therefore, enhanced low-energy optical absorption in the doped materials is the result of the introduction of the Cr-3d impurity states and their growing role. Spin polarization of the Cr-3d states is a clear indicator of the modification of the electronic structure caused by Cr substitution and agrees with the calculated magnetic moment. Thus, DOS/PDOS, band structure, and optical properties give a consistent physical picture in which the

introduction of Cr causes the formation of localized electronic states, narrowing of the band gap, and, as a result, an enhanced optical response at lower photon energies.

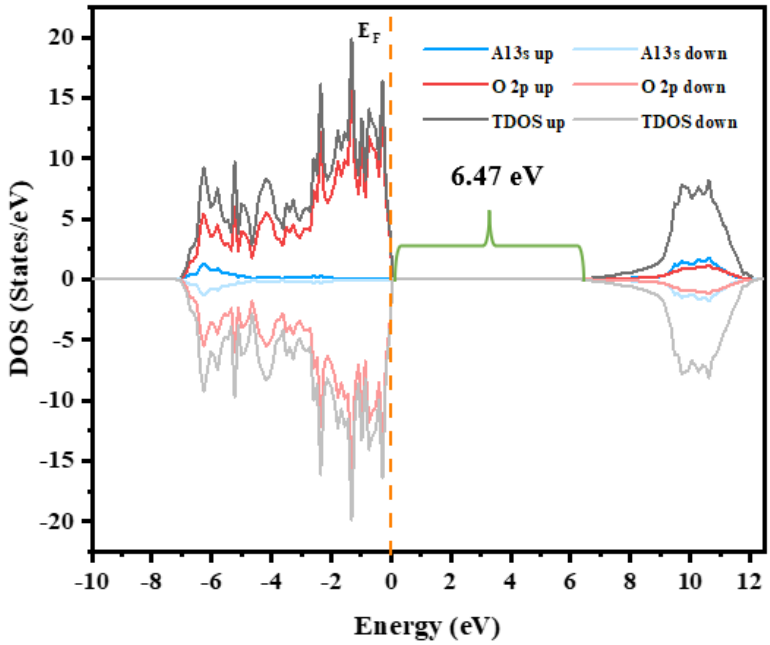


Figure 5: Total and partial density of states (TDOS/PDOS) of pristine α-Al_2O_3.

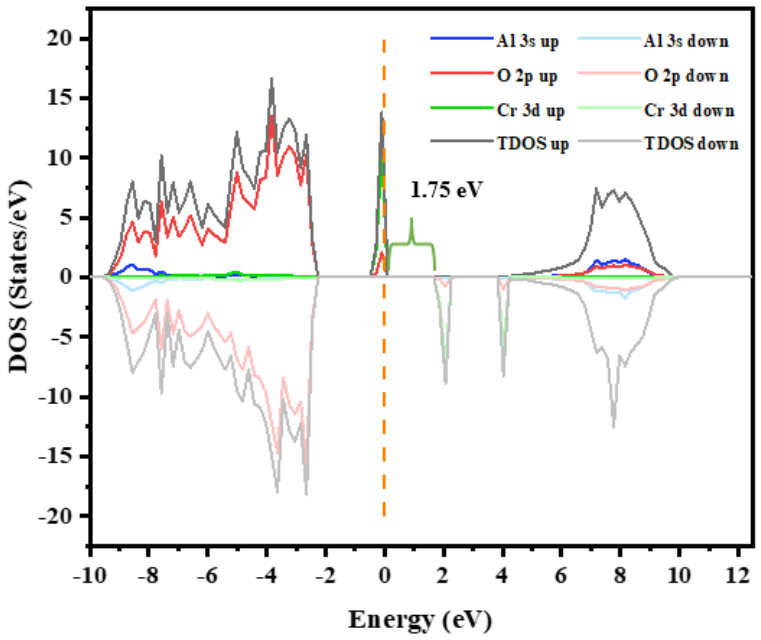


Figure 6: Total and partial density of states (TDOS/PDOS) of 8.33% substitutional Cr-doped α-Al_2O_3.

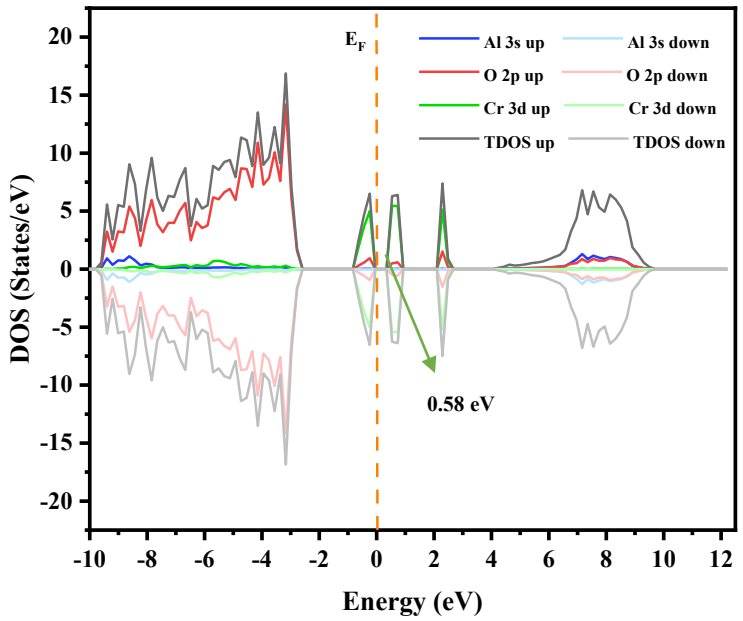


Figure 7: Total and partial density of states (TDOS/PDOS) of 16.66% substitutional Cr-doped α-Al_2O_3.

3.2.2 Dielectric constant

The dielectric function describes the interaction between photons and electrons and provides important information about interband electronic transitions within a material. To describe the optical response of the system, the complex dielectric function is expressed as $\varepsilon(\omega) = \varepsilon_1(\omega) + i\varepsilon_2(\omega)$, where $\varepsilon_1(\omega)$ and $\varepsilon_2(\omega)$ denote the real and imaginary parts, respectively [65]. The real part, $\varepsilon_1(\omega)$, is associated with the polarization and energy-storage characteristics of the material, whereas the imaginary part, $\varepsilon_2(\omega)$, represents the optical absorption resulting from electronic transitions between occupied and unoccupied states. Therefore, $\varepsilon_2(\omega)$ is directly related to the probability of electron excitation from the valence band to the conduction band under incident photon irradiation. In the present study, particular attention is given to the variation of the imaginary dielectric function within the energy range of 1.63–3.10 eV. The dielectric function serves as an important link between the electronic band structure and the optical behavior of crystalline materials [66]. Both $\varepsilon_1(\omega)$ and $\varepsilon_2(\omega)$ are obtained from calculations of the momentum matrix elements between occupied and unoccupied electronic states [67, 68]. From a quantum-mechanical perspective, photon absorption induces electronic transitions from lower-energy occupied states to higher-energy unoccupied states, generating optical spectra associated with the electronic density of states. In addition, several optical parameters, such as the absorption coefficient $\alpha(\omega)$, can be derived from the calculated dielectric function using density functional theory methods [69, 70].

$$\varepsilon_2 = \frac{C_1}{\omega^2}\sum_{V.C}\int_{BZ} d^3K \frac{2}{(2\pi)} |e \cdot M_{CV}(K)|^2 \delta[E_C(K) - E_V(K) - \hbar\omega] \quad (1)$$

$$\varepsilon_1 = 1 + C_2 \sum_{V.C} \int_{BZ} d^3K \frac{2}{(2\pi)} \frac{|e \cdot M_{CV}(K)|^2}{[E_c(K) - E_V(K)]} \frac{\hbar^3}{[E_C(K) - E_V(K)]^2 - \hbar^2\omega^2} \quad (2)$$

$$\alpha(\omega) = \sqrt{2}\omega \left[\sqrt{\varepsilon_1^2(\omega) + \varepsilon_2^2(\omega)} - \varepsilon_1(\omega) \right]^{\frac{1}{2}} \quad (3)$$

In the above equation, VB and CB denote the valence band and conduction band, respectively, while BZ represents the first Brillouin zone. The quantities k, $\hbar$, and ω correspond to the electron wave vector, reduced Planck constant, and angular frequency, respectively. The symbol δ denotes the Dirac delta function, and $|M_{CV}(k)|^2$ represents the squared momentum transition matrix element. $E_C(k)$ and $E_V(k)$ correspond to the energy levels of the conduction-band minimum (CBM) and valence-band maximum (VBM), respectively, whereas C_1 and C_2 are constants.

The real part of the dielectric function, $\varepsilon_1(\omega)$, for both pure and Cr-doped α-Al_2O_3 at different concentrations is presented in Figure 8(a). The results indicate that $\varepsilon_1(\omega)$ increases in the low-energy region, where the dielectric constant rises from approximately 3 to 5 with increasing Cr concentration. The positive values of $\varepsilon_1(\omega)$ indicate a predominantly dielectric response in this energy range; transparency additionally depends on the magnitude of the absorption or $\varepsilon_2(\omega)$ [71]. In addition, $\varepsilon_1(\omega)$ provides insight into the interaction between the material and incident electromagnetic radiation. It is also observed that the first peak of $\varepsilon_1(\omega)$ shifts toward lower energies with a slight reduction in intensity after Cr doping. At higher photon energies, $\varepsilon_1(\omega)$ increases again to larger positive values, indicating modifications in the electronic polarization response due to the introduction of Cr-induced electronic states.

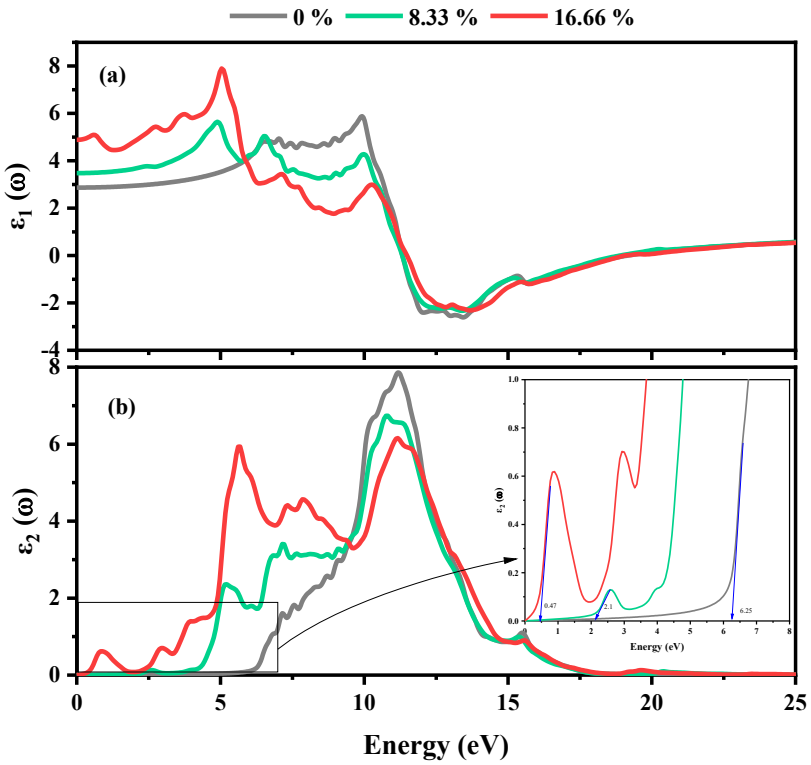


Figure 8: (a) Real part, $\varepsilon_1(\omega)$, and (b) imaginary part, $\varepsilon_2(\omega)$, of the dielectric function of pristine and Cr-doped α-Al_2O_3 at 8.33% and 16.66% Cr concentrations.

Figure 8(b) presents the imaginary part of the dielectric function, $\varepsilon_2(\omega)$, for pure and Cr-doped α-Al_2O_3 at different concentrations. The peaks in $\varepsilon_2(\omega)$ correspond to optical transitions between the valence band (VB) and conduction band (CB), indicating the photon energies at which electrons absorb energy and transition to higher-energy states. Therefore, the analysis of $\varepsilon_2(\omega)$ provides important insight into the optical behavior and electronic transitions of the material.

For pure α-Al_2O_3, the spectrum exhibits two dominant peaks located at approximately 11 eV and 15.5 eV. The first peak mainly originates from transitions of electrons from O-2p and Al-3p states

in the upper valence band to Al-3s, Al-3p, and O-2p states in the conduction band. The second peak is associated with transitions involving deeper valence-band states, particularly O-2s and Al-3s orbitals. After Cr doping at 8.33%, a new peak appears around 5 eV, these features can be associated with transitions involving O-2p/Al-derived occupied states and Cr-3d-derived unoccupied states. The emergence of these impurity-related states contributes to the observed band-gap reduction. In this case, $\varepsilon_2(\omega)$ exhibits two main peaks, with a reduction in the intensity of the higher-energy peak. When the Cr concentration increases to 16.66%, three prominent peaks are observed. The additional peak is attributed to transitions involving Cr-3d states introduced within the band gap. These results indicate that increasing Cr concentration modifies the electronic structure and enhances optical absorption in the lower-energy region.

The reduction in the band gap and the enhanced optical absorption in Cr-doped α-Al_2O_3 may qualitatively suggest improved light-harvesting capability. However, definitive conclusions regarding photocatalytic performance cannot be established because band-edge alignment, redox-potential analysis, and charge-carrier recombination studies were not performed in the present work. Therefore, any discussion of photocatalytic applicability should be regarded only as qualitative and preliminary.

Furthermore, the refractive index $n(\omega)$ and extinction coefficient $k(\omega)$ were investigated to better understand the interaction between electromagnetic radiation and the material. The refractive index describes the propagation and bending of light within the material, whereas the extinction coefficient is related to optical absorption and attenuation [72,73]. Figure 9(a) shows that the refractive index increases with increasing photon energy and Cr concentration in the energy range of approximately 2–9 eV. In the infrared region, $n(\omega)$ remains nearly constant, forming a plateau-like behavior. Figure 9(b) presents the extinction coefficient $k(\omega)$, the enhanced extinction

coefficient in the low-energy region is consistent with stronger optical attenuation associated with the Cr-induced electronic states due to the introduction of impurity states. At higher photon energies, the curves for pure and doped systems become similar, suggesting comparable absorption behavior in that region. Overall, Cr incorporation modifies the optical response of α-Al_2O_3 through changes in the electronic structure and optical-transition characteristics.

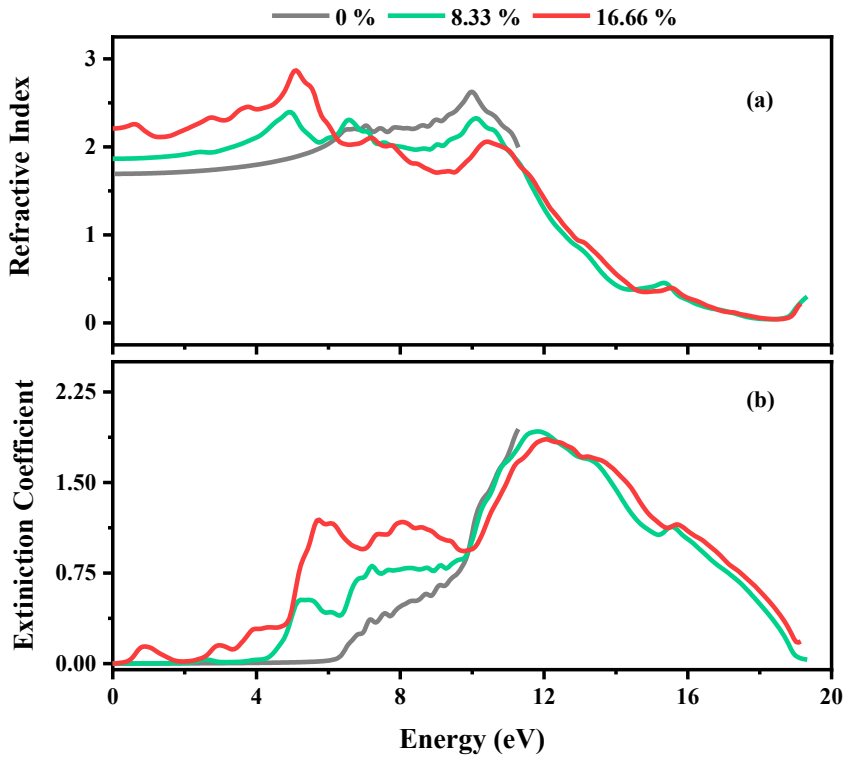


Figure 9: (a) Refractive index, n(ω), and (b) extinction coefficient, k(ω), of pristine and Cr-doped α-Al_2O_3 at 8.33% and 16.66% Cr concentrations.

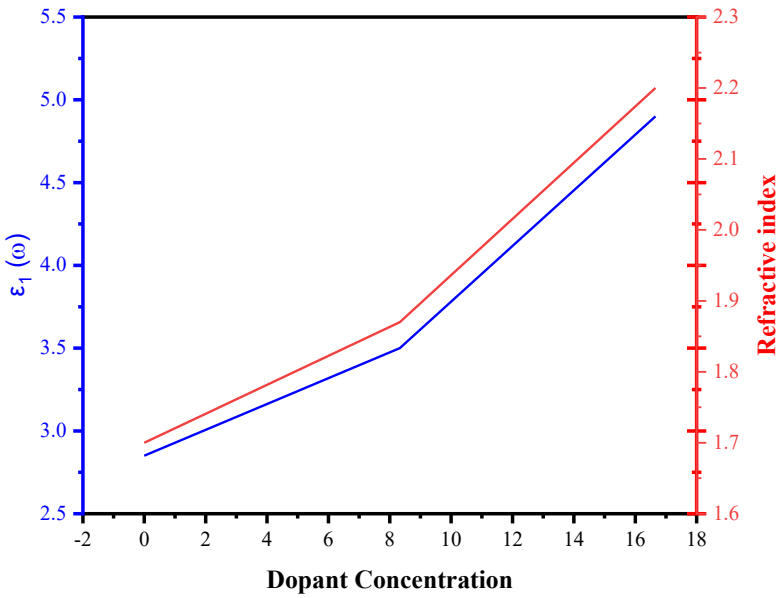


Figure 10: Static dielectric constant, $\varepsilon_1(0)$, and refractive index, n(0), as a function of Cr concentration in α-Al_2O_3.

The impact of Cr doping on the static dielectric constant $\varepsilon_1(0)$ and the n of α-Al_2O_3 is shown in Figure 10. This figure shows the static dielectric constant, $\varepsilon_1(0)$, and refractive index, n, of pristine and Cr-doped α-Al_2O_3. Both $\varepsilon_1(0)$ and n increase with increasing Cr concentration, indicating enhanced electronic polarizability and a modified interaction with electromagnetic radiation. This behavior is consistent with the reduction of the calculated band gap and the associated changes in the electronic structure. In the low-frequency limit, the refractive index is approximately related to the dielectric constant by $n^2 \approx \varepsilon_1(0)$, assuming negligible absorption.

3.2.3 Absorption coefficient

The calculated absorption coefficient provides information about the photon-energy dependence of optical absorption and is closely related to the electronic structure. The capability of the material to absorb different numbers of photons at different energies is determined by the absorption coefficient. The absorption coefficient study reveals crucial information about the band structure of material. The absorption edge was estimated from the onset of significant optical absorption in the calculated absorption spectrum where the absorption reaches zero as shown in figure 10. The figure also shows that the absorption edge of pure α-Al_2O_3 is 6.47 eV as predicted by the band structure. However, for the Cr-doped α-Al_2O_3, the absorption edge is at 1.75 eV and 0.57 eV for 8.33% and 16.66% of the doping concentration, respectively, as observed in Figure 12 and Figure 13. The pronounced increase in the absorption coefficient for the visible and NIR regions of the spectra for the doped samples is due to the introduction of the localized Cr-3d states in the band structure. The enhanced visible-light absorption indicates that Cr incorporation modifies the spectral range of optical response; however, assessment of solar-energy conversion requires further band-alignment, carrier-transport, and device-level studies [74].

The observed reduction of the band gap and electronic structure modification by Cr doping agrees with the general trends reported recently in first-principles studies of functional materials. Several DFT studies have shown that compositional engineering, such as elemental substitution and defect incorporation, is an effective strategy to tune the electronic and optical properties of wide-band-gap materials, by introducing localized electronic states and changing the distribution of valence and conduction bands. In particular, recent studies have revealed that modifications in chemical composition can profoundly affect the optical absorption, dielectric response, and charge-transfer properties, thus improving the applicability of materials in optoelectronic and energy-related

applications [16-19]. In the same vein, recent theoretical studies on photocatalytic materials have highlighted that band-gap engineering through electronic structure modification plays a key role in improving visible-light utilization and optimizing the functional performance of semiconductor materials [15]. The mechanism of tailoring the electronic structure via controlled compositional modification is consistent with these recent DFT investigations, although the present work focuses on Cr-doped α-Al_2O_3 rather than hydride or double-perovskite systems.

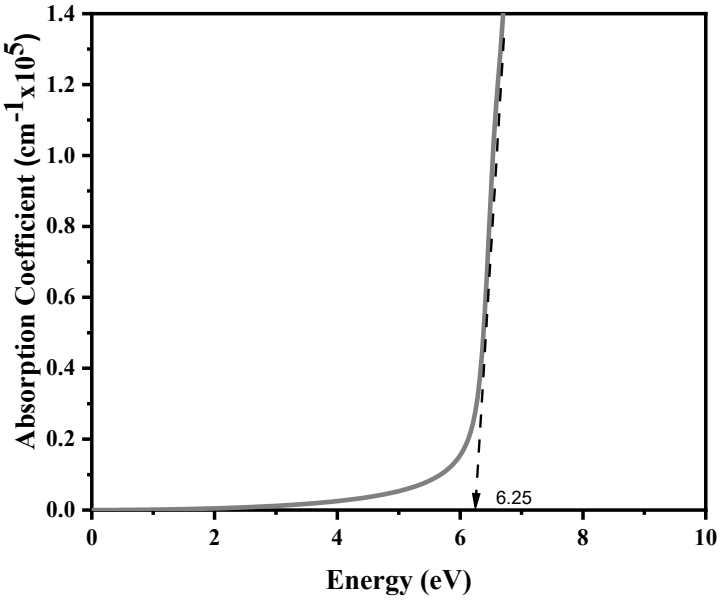


Figure 11: Calculated absorption coefficient, α(ω), of pristine α-Al_2O_3.

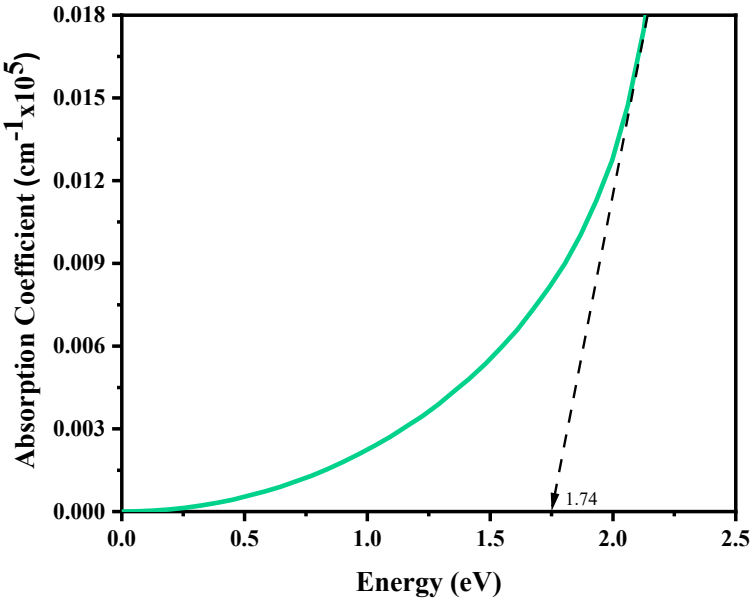


Figure 12: Calculated absorption coefficient, α(ω), of 8.33% substitutional Cr-doped α-Al_2O_3.

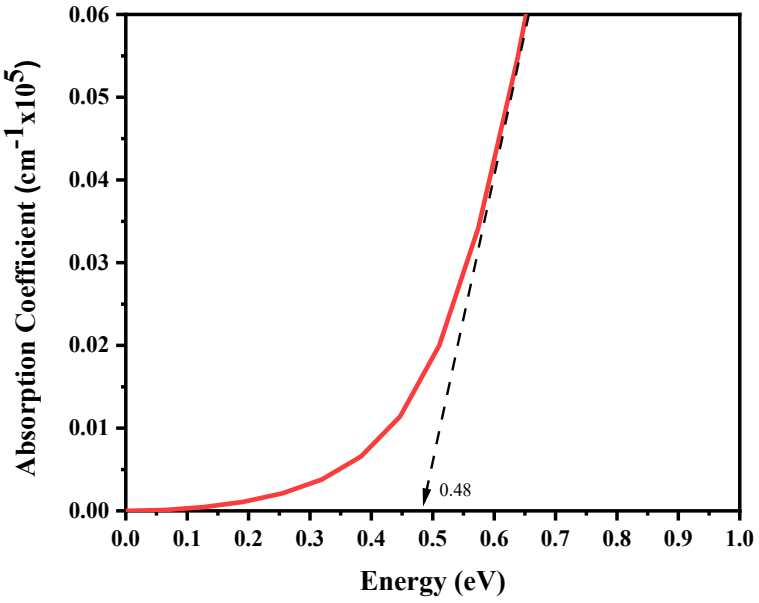


Figure 13: Calculated absorption coefficient, α(ω), of 16.66% substitutional Cr-doped α-Al_2O_3.

3.2.4 Tauc Method

The interband absorption model is of prime importance for understanding the electronic transitions that occur in the band gap of the material. This model can be used to support the inference from the E-K diagram. According to the theory of interband absorption, photons can carry electrons from the VB's top to the available states at the bottom of the CB. This is referred to as an interband transition, and the optical band gap of the material can be determined using the formula given below [75]

$$\alpha h\nu = A\left(h\nu - E_g\right)^{\gamma} \qquad (4)$$

In this instance, the electronic transitions determine γ, which is a constant. For permitted direct transitions, the value of γ is 1/2, and for prohibited direct transitions, it is 3/2. Additionally, for permitted indirect transitions, γ is 2, while for prohibited indirect transitions, it is 3. Figure 14 shows all possible transitions for pure α-Al_2O_3. The linear portion of each graph that was projected to the energy axis was used to estimate the E_g values for all kinds of transitions. As may be observed, the band structure is matched by an allowable direct transition in pure α-Al_2O_3 as shown in figure 14(a).

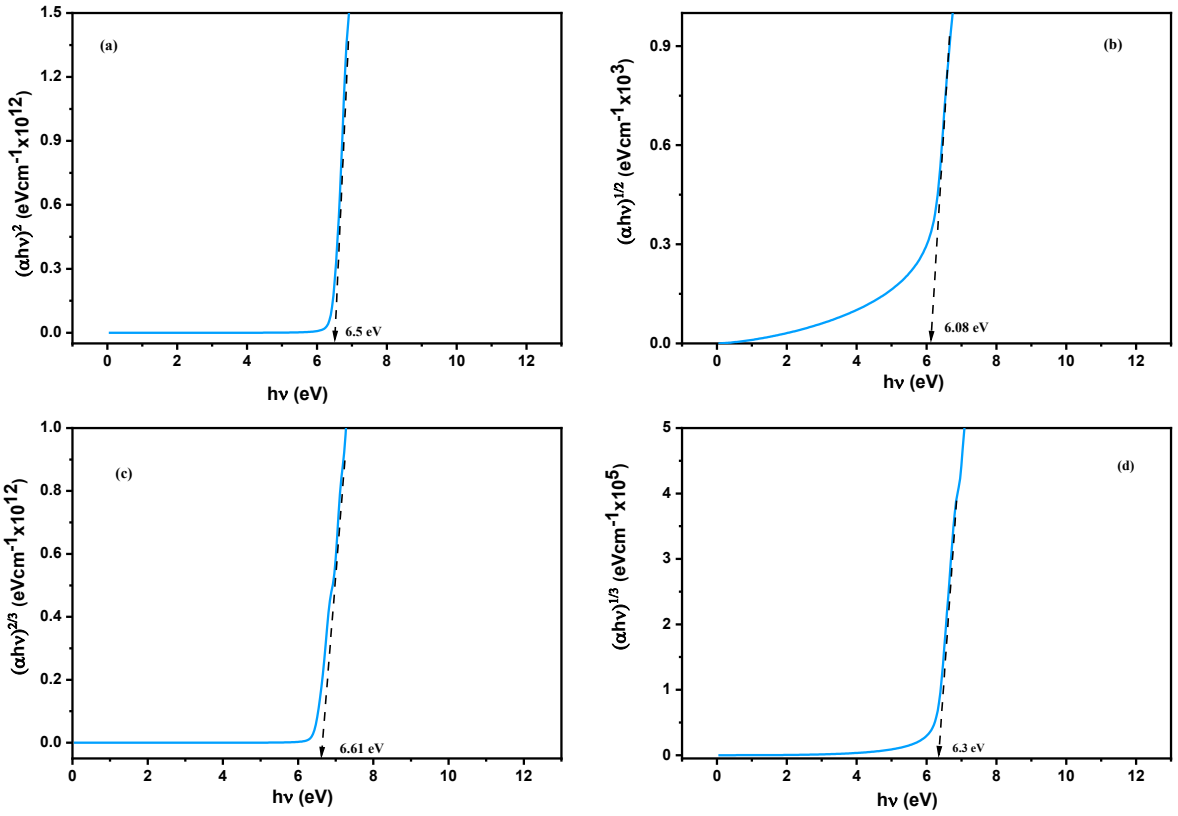


Figure 14: Tauc plots for pristine α-Al_2O_3 considering (a) allowed direct, (b) allowed indirect, (c) forbidden direct, and (d) forbidden indirect transitions.

The Tauc plots for Cr-doped α-Al_2O_3 are depicted in Figures 15 and 16. It should be mentioned that the band gap values estimated from Tauc plots show reasonable agreement with corresponding values estimated from the E-k diagrams, and thus confirm the consistency between the optical and electronic properties of the materials studied. Based on the electronic band structure results, pristine α-Al_2O_3 exhibits a direct fundamental transition, 8.33% Cr-doped Al_2O_3 shows an indirect fundamental transition (figure 15(b)), and 16.66% Cr-doped Al_2O_3 exhibits a direct fundamental transition (figure 16(a)). The Tauc plot analyses are consistent with the above transition types and support band gap narrowing. The correct Tauc exponent value was chosen depending on the

transition type determined from the electronic band structure. This technique was employed alongside the absorption measurement in order to evaluate the absorption threshold energy. Since localized states induced by chromium could cause additional transitions, the Tauc results should be taken into account carefully and cannot be regarded as an independent measurement of the fundamental band gap.

It should be noted that tauc analysis should be considered a complementary optical analysis, rather than an independent calculation of the basic electronic band gap. The point here is that the addition of Cr-3d localized impurity states to the α-Al_2O_3 system makes it possible to form additional electronic states in the host band gap, resulting in optical transitions that are not necessarily related to a classical valence-conduction band transition. In this case, the band structure is considered to be a basic tool for determining the transition character, while the Tauc plots allow to determine the value of optical absorption threshold and analyze the systematic change of optical gap with the concentration of Cr. The transition type determined based on the band structure is in good agreement with the Tauc analysis: pristine α-Al_2O_3 shows the direct transition, 8.33% Cr-doped sample – the indirect transition, and 16.66% Cr-doped sample – the direct transition. Nevertheless, due to the contribution of localized Cr-3d states to low energy optical excitations and the fact that GGA-PBE gives an underestimated value for the absolute band gap, these Tauc estimated values have to be treated more as a qualitative estimation.

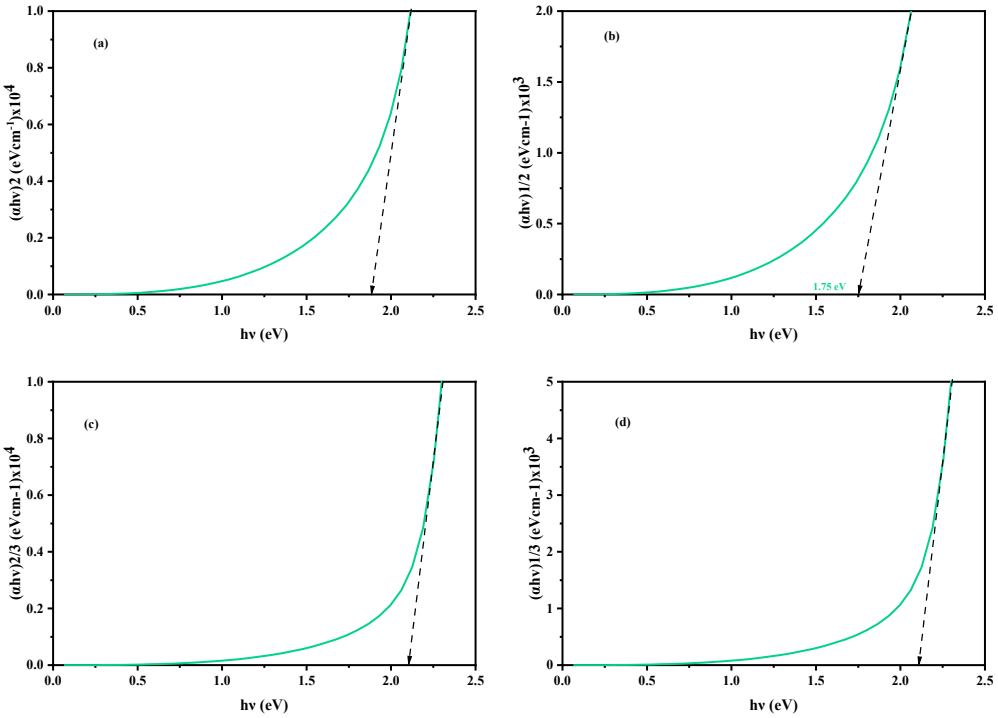


Figure 15: Tauc plots for 8.33% substitutional Cr-doped α-Al_2O_3 considering (a) allowed direct, (b) allowed indirect, (c) forbidden direct, and (d) forbidden indirect transitions.

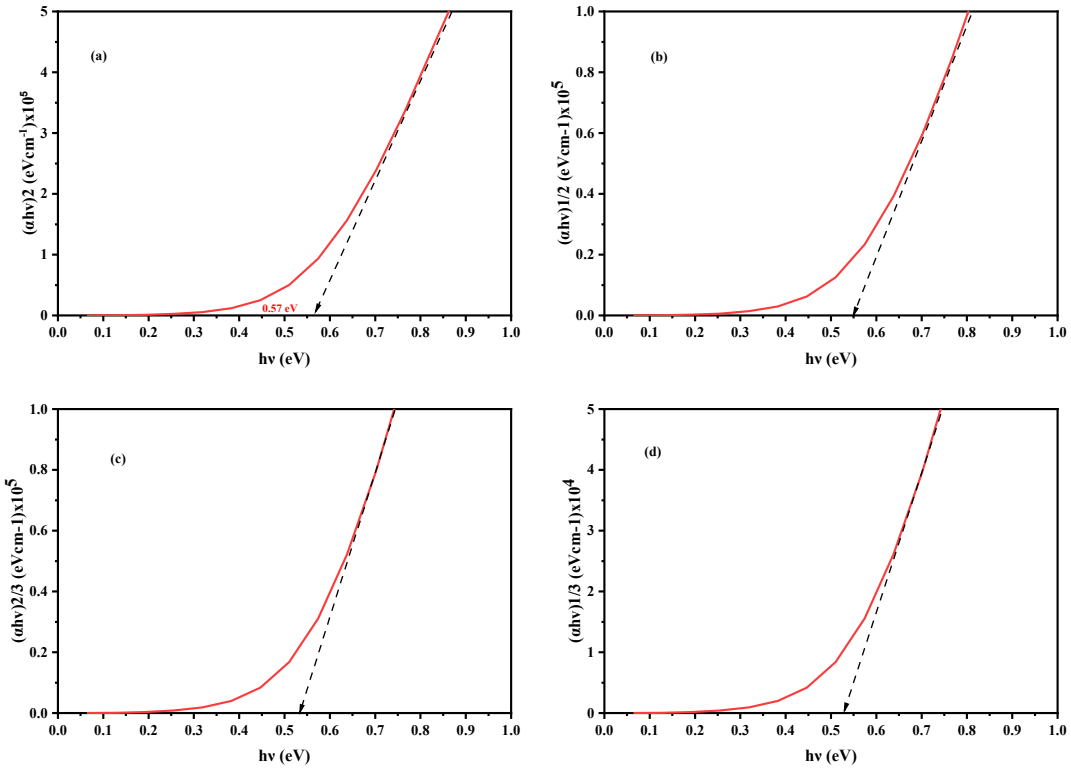


Figure 16: Tauc plots for 16.66% substitutional Cr-doped α-Al_2O_3 considering (a) allowed direct, (b) allowed indirect, (c) forbidden direct, and (d) forbidden indirect transitions.

Table 3 shows a list of calculated band gap energies for pure and Cr-doped α-Al_2O_3 structures using different approaches, such as electronic band structure, dielectric loss spectrum, absorption edge, and Tauc methods. In the case of pure ($Al_{12}O_{18}$), it is observed that the calculated band gap using the electronic band structure is in close agreement with those calculated using optical approaches such as dielectric loss spectrum, absorption edge, and Tauc methods. This is true for other structures, such as doped systems ($Al_{11}CrO_{18}$ and $Al_{10}Cr_2O_{18}$), where a close agreement is observed among different approaches for calculating the optical band gap. Among all these approaches, The Tauc-derived optical gaps are broadly consistent with the corresponding band-edge energies obtained from the electronic-structure calculations, supporting the observed

systematic band-gap reduction with increasing Cr concentration. It is found that as the concentration is increased the band gap decreases, indicating the introduction of impurity levels in the band structure, which increases the optical absorption in the low energy region. It is important to emphasize the fact that the GGA-PBE function tends to underestimate the absolute values of band gaps for semiconducting and insulating substances. Therefore, the predicted values of band gaps, especially the extremely small value of 0.57 eV in the case of Cr-doped α-Al_2O_3 at 16.66%, should be treated cautiously and cannot be considered as an accurate quantitative value of the experimental band gap. However, the systematic decrease in the values of the calculated band gaps from 6.47 eV in the pure α-Al_2O_3 to 1.75 eV and 0.57 eV with the increase of Cr content demonstrates the significant influence of Cr on the electronic structure of the substance. It means that the current calculations using the GGA-PBE function can provide a more accurate description of the qualitative trend of band-gap reduction than the quantitative values of the band gaps.

Table 3: Calculated band-gap energies of pristine and Cr-doped α-Al_2O_3 obtained from electronic band-structure, dielectric-loss, absorption-edge, and Tauc analyses.

Structure	Band Structure (eV)	Dielectric Loss (eV)	Absorption Edge (eV)	Tauc Method (eV)
Al_2O_3	6.47	6.25	6.25	6.30
Cr: α-Al_2O_3 (8.33%)	1.75	2.10	1.74	1.75
Cr: α-Al_2O_3 16.66%)	0.57	0.47	0.48	0.57

4. Conclusion

In conclusion, the current study made use of first-principle DFT calculations based on the GGA-PBE method using the VASP software package in order to examine the influence of Cr dopant on the electronic and optical properties of α-Al_2O_3 for concentrations 8.33% and 16.66%. The

computational results show significant systematic reduction of the band gap value with an increase in Cr concentration, namely, the value reduces from 6.47 eV in case of pristine α-Al_2O_3 to 1.75 eV and 0.57 eV for Cr concentrations of 8.33% and 16.66%, respectively. Nevertheless, the exact values of the band gaps need to be taken with a grain of salt and cannot be regarded as the quantitative estimation of the band gap measured experimentally. These band gaps rather confirm the qualitative tendency of the narrowing of the band gap and the presence of Cr-related impurities inside the host band gap. The limitations related to the use of GGA-PBE exchange-correlation functional, high Cr content, and periodic supercell assumption might have an effect on absolute band gap values. Thus, more sophisticated calculations using hybrid-functional or many-body methods, along with experiments, are needed in order to obtain quantitative information about band gaps. In this context, the findings obtained within the scope of this work should be viewed rather as qualitative proof of significant impact of Cr doping on electronic and optical properties of α-Al_2O_3. Still, the found band gap reduction and increased absorption in the visible region give some hints concerning the application of α-Al_2O_3 in optoelectronics. It is important to point out that although negative formation energy values have been calculated for Cr-doped structures which prove their energetic advantage in terms of Cr doping under given chemical potentials, these findings do not provide any information regarding overall structural stability. No mechanical stability test has been conducted since there are no elastic constant values available, and it is impossible to prove the dynamical stability of the structures since phonon dispersion calculations have not been made. Thus, the current study should not be considered as the one proving the mechanical and dynamical stability of the Cr-doped systems.

Acknowledgements

The authors gratefully acknowledge all facilities to carry out this research from the University of Sulaimani and the University of Jouf.

Conflicts of Interest

The authors declare that they have no known competing financial interests or personal relationships that could have appeared to influence the work reported in this paper.

Data Availability Statement

The data underlying this article will be shared on reasonable request from the corresponding author.

Funding Declaration

There are no funds to declare

Author contributions

Taha Y. Ahmed contributed to the computational methodology and wrote the original manuscript. **Shujahadeen B. Aziz** contributed to conceptualization, supervision, funding acquisition, project administration, and manuscript editing. All authors read and approved the final version of the manuscript

References

[1] M. Farahmandjou, A. Khodadadi, and M. Yaghoubi, "Low concentration iron-doped alumina (Fe/Al_2O_3) nanoparticles using co-precipitation method," Journal of Superconductivity and Novel Magnetism, vol. 33, no. 11, pp. 3425–3432, 2020.

[2] G. B. Grad, E. R. Gonzalez, J. Torres-Diaz, and E. V. Bonzi, "A DFT study of ZnO, Al_2O_3 and SiO2; combining X-ray spectroscopy, chemical bonding and Wannier functions," Journal of Physics and Chemistry of Solids, vol. 168, p. 110788, 2022.

[3] E. O. Filatova and A. S. Konashuk, "Interpretation of the changing the band gap of Al_2O_3 depending on its crystalline form: connection with different local symmetries," The Journal of Physical Chemistry C, vol. 119, no. 35, pp. 20755–20761, 2015.

[4] Y. Ji and J. A. Yeomans, "Microstructure and mechanical properties of chromium and chromium/nickel particulate reinforced alumina ceramics," Journal of Materials Science, vol. 37, no. 24, pp. 5229–5236, 2002.

[5] Y. L. Zhu, S. Liu, X. K. Zhang, and Y. Xiang, “Effects of Cr3+ concentration on the crystallinity and optical properties of Cr-doped Al_2O_3 powders by solid-state reaction method,” in IOP Conference Series: Materials Science and Engineering, vol. 382, no. 2, p. 022037, 2018.

[6] T. Y. Ahmed, S. B. Aziz, and E. M. Dannoun, “New photocatalytic materials based on alumina with reduced band gap: A DFT approach to study the band structure and optical properties,” Heliyon, vol. 10, no. 5, 2024.

[7] C. B. Samantaray, H. Sim, and H. Hwang, “First-principles study of electronic structure and electron energy-loss-spectroscopy (EELS) of transition-metal aluminates as high-k gate dielectrics,” Applied Surface Science, vol. 242, no. 1–2, pp. 121–128, 2005.

[8] A. Kadari, S. E. Rezak, K. Kassi, and M. Chehairi, “Investigation of the optical and structural properties of Cr3+-doped Al_2O_3 and Zn Al_2O_4 nanoparticles synthesized by sol–gel method,” Nanosistemi, Nanomateriali, Nanotehnologii, vol. 20, no. 2, 2022.

[9] R. C. R. Santos, E. Longhinotti, V. N. Freire, R. B. Reimberg, and E. W. S. Caetano, “Elucidating the high-k insulator α- Al_2O_3 direct/indirect energy band gap type through density functional theory computations,” Chemical Physics Letters, vol. 637, pp. 172–176, 2015.

[10] T. V. Perevalov, A. V. Shaposhnikov, V. A. Gritsenko, H. Wong, J. H. Han, and C. W. Kim, “Electronic structure of α- Al_2O_3: Ab initio simulations and comparison with experiment,” JETP Letters, vol. 85, no. 3, pp. 165–168, 2007.

[11] S. J. Mousavi, M. R. Abolhassani, S. M. Hosseini, and S. A. Sebt, “Comparison of electronic and optical properties of the α and κ phases of alumina using density functional theory,” Chinese Journal of Physics, vol. 47, no. 6, pp. 862–873, 2009.

[12] L. Maaza, F. Djafri, A. Belmokhtar, and A. Benyoucef, “Evaluation of the influence of Al_2O_3 nanoparticles on the thermal stability and optical and electrochemical properties of PANI-derived matrix reinforced conducting polymer composites,” Journal of Physics and Chemistry of Solids, vol. 152, p. 109970, 2021.

[13] Y. Ji and J. A. Yeomans, “Processing and mechanical properties of Al_2O_3–5 vol.% Cr nanocomposites,” Journal of the European Ceramic Society, vol. 22, no. 12, pp. 1927–1936, 2002.

[14] A. F. Alamouti, M. Nadafan, Z. Dehghani, M. M. Ara, and A. V. Noghreiyan, “Structural and optical coefficients investigation of γ- Al_2O_3 nanoparticles using Kramers-Kronig relations and Z–scan technique,” Journal of Asian Ceramic Societies, vol. 9, no. 1, pp. 366–373, 2021.

[15] Errahoui, H., Karouchi, M., Ejjabli, A., Laassouli, A., El Haji, A., Lachtioui, Y. and Bajjou, O., 2025. Photocatalytic properties of XH_2 (X= Ca, Ba, Mg, and Sr): unlocking potential for sustainable energy and environmental applications. Catalysis Letters, 155(11), p.359.

[16] Laassouli, A., Karouchi, M., Ejjabli, A., Haji, A.E., Errahoui, H., Lachtioui, Y. and Bajjou, O., 2026. Novel Insights into the Electric Field-Driven Electronic and Optical Behavior of K_2AgSbI_6 via DFT. Journal of Electronic Materials, 55(2), pp.2149-2161.

[17] Laassouli, A., Karouchi, M., Ejjabli, A., Errahoui, H., Haji, A.E., Lachtioui, Y. and Bajjou, O., 2026. Tuning optoelectronic properties in $BaNaH_3X$ (X= Ni, Pd, Pt) perovskite hydrides: a DFT-based analysis. Journal of Molecular Modeling, 32(2), p.39.

[18] Laassouli, A., Karouchi, M., Ejjabli, A., Errahoui, H., El Haji, A., Lachtioui, Y. and Bajjou, O., 2026. Structural, mechanical, electronic, and optoelectronic properties of wide-band-gap hydride perovskite $BaNaH_3Pt$ from hybrid density functional theory. Next Materials, 11, p.101803.

[19] Laassouli, A., Karouchi, M., Ejjabli, A., Haji, A.E., Errahoui, H., Rahmani, K., Lachtioui, Y. and Bajjou, O., 2026. Halide-driven tuning of structural, electronic, and optical properties in lead-free K_2AgSbX_6 (X= I, Br, Cl) double perovskites: a DFT study. Journal of Molecular Modeling, 32(4), p.94.

[20] M. T. Iqbal et al., “Next-generation materials discovery using DFT: functional innovation,” Sol. Energy Catal. Eco Toxic. Model. Sch. J. Eng. Tech., vol. 7, pp. 454–486, 2025.

[21] G. A. Alharshan et al., “Optical band gap tuning, DFT understandings, and photocatalysis performance of ZnO nanoparticle-doped Fe compounds,” Materials, vol. 16, no. 7, p. 2676, 2023.

[22] F. T. Geldasa, F. B. Dejene, M. A. Kebede, F. G. Hone, and E. T. Jira, “Density functional theory study of chlorine, fluorine, nitrogen, and sulfur doped rutile TiO_2 for photocatalytic application,” Scientific Reports, vol. 15, no. 1, p. 3390, 2025.

[23] F. T. Geldasa and F. B. Dejene, “Influence of fluorine doping on rutile TiO_2 nanostructures for visible-light-driven photocatalysis: A DFT+U study,” Nanomaterials, vol. 15, no. 9, p. 694, 2025.

[24] N. Kelaidis, Y. Panayiotatos, and A. Chroneos, “Chalcogen doping in SnO_2: A DFT investigation of optical and electronic properties for enhanced photocatalytic applications,” Materials, vol. 17, no. 16, p. 3910, 2024.

[25] S. Dash, S. Mohanty, D. Behera, S. K. Mohanty, and G. Palai, “Band gap engineering and optical response of $SrSiO_3$ perovskite for high-efficiency photonic applications,” MRS Advances, vol. 10, no. 19, pp. 2267–2274, 2025.

[26] S. Dash, D. Behera, S. K. Mohanty, G. Palai, and I. Mohanty, “Unveiling the potential of lead-free $KInBr_3$ and $RbInBr_3$ perovskites: A breakthrough in optoelectronic and photovoltaic performance through DFT (HSE hybrid functional) and SCAPS-1D simulations,” Phase Transitions, vol. 97, no. 11–12, pp. 826–845, 2024.

[27] S. Dash, D. Behera, S. Mohanty, J. Panda, and G. Palai, “Comprehensive investigations on the optoelectronic properties of lead-free $K_2InSbCl_6$ compound,” Next Research, p. 100607, 2025.

[28] S. Dash, S. Mohanty, and G. Palai, “First-principles insights into structural, electronic, elastic, and optical behavior of $AlGeX_3$ (X = Cl, Br) perovskites,” Russian Journal of Inorganic Chemistry, vol. 70, no. 7, pp. 1100–1108, 2025.

[29] S. Dash, D. Behera, I. Mohanty, A. Priyambada, and S. K. Sahoo, “From electronic structure to device performance: A DFT and SCAPS-1D investigation of $AlSnX_3$ (X = Cl, Br) perovskites,” Inorganic Chemistry Communications, p. 116106, 2025.

[30] J. Hafner, “Ab-initio simulations of materials using VASP: Density-functional theory and beyond,” Journal of Computational Chemistry, vol. 29, no. 13, pp. 2044–2078, 2008.

[31] J. P. Perdew et al., “Restoring the density-gradient expansion for exchange in solids and surfaces,” Physical Review Letters, vol. 100, no. 13, p. 136406, 2008.

[32] V. Wang, N. Xu, J. C. Liu, G. Tang, and W. T. Geng, “VASPKIT: A user-friendly interface facilitating high-throughput computing and analysis using VASP code,” Computer Physics Communications, vol. 267, p. 108033, 2021.

[33] H. J. Monkhorst and J. D. Pack, “Special points for Brillouin-zone integrations,” Physical Review B, vol. 13, no. 12, p. 5188, 1976.

[34] J. D. Pack and H. J. Monkhorst, “Special points for Brillouin-zone integrations—A reply,” Physical Review B, vol. 16, no. 4, p. 1748, 1977.

[35] R. H. French, “Electronic band structure of Al_2O_3, with comparison to AlON and AlN,” Journal of the American Ceramic Society, vol. 73, no. 3, pp. 477–489, 1990.

[36] R. Zhao, Q. Fan, R. Yang, Y. Song, X. Yu, and S. Yun, “Exploration of stable novel Al_2O_3 by high-throughput calculation screening and density functional theory,” SSRN Electronic Journal, 2022. doi: 10.2139/ssrn.4132126.

[37] Y. N. Xu and W. Y. Ching, “Self-consistent band structures, charge distributions, and optical-absorption spectra in MgO, α- Al_2O_3, and $MgAl_2O_4$,” Physical Review B, vol. 43, no. 5, p. 4461, 1991.

[38] M. Choi, A. Janotti, and C. G. Van de Walle, “Native point defects and dangling bonds in α-Al2O3,” Journal of Applied Physics, vol. 113, no. 4, 2013.

[39] D. Nouar, A. Hamdi, A. Benghia, and M. E. Sarhani, “First-principles investigation of structural, electronic, and optical transitions in $FexZr1{-}xO_2$ solid solutions,” Applied Sciences, vol. 15, no. 18, p. 10224, 2025.

[40] M. E. Laamari, A. Cheknane, A. Benghia, and H. S. Hilal, “Optimized opto-electronic and mechanical properties of orthorhombic methylammonium lead halides ($MAPbX_3$) (X = I, Br and Cl) for photovoltaic applications,” Solar Energy, vol. 182, pp. 9–15, 2019.

[41] A. Benghia, T. Dahame, and B. Bentria, “Ab initio investigation of the structural and optoelectronic properties of aluminum thiophosphate $AlPS_4$,” in JOURNÉES D’ÉTUDES SUR LES MATÉRIAUX (JEM 2014), 2014.

[42] K. Parlinski, Z. Q. Li, and Y. Kawazoe, “First-principles determination of the soft mode in cubic ZrO_2,” Physical Review Letters, vol. 78, no. 21, p. 4063, 1997.

[43] J. Singleton, Band Theory and Electronic Properties of Solids, vol. 2. Oxford, U.K.: Oxford University Press, 2001.

[44] C. Kittel and P. McEuen, Introduction to Solid State Physics. Hoboken, NJ, USA: John Wiley & Sons, 2018.

[45] T. Dietl, “A ten-year perspective on dilute magnetic semiconductors and oxides,” Nature Materials, vol. 9, no. 12, pp. 965–974, 2010.

[46] G. Pari, A. Mookerjee, and A. K. Bhattacharya, “Study of α- Al_2O_3 and the role of Y in $YAlO_3$ and Y3Al5O12 by first-principles electronic structure calculations,” Physica B: Condensed Matter, vol. 353, no. 3–4, pp. 192–200, 2004.

[47] M. Wang, X. Huang, Z. Du, and Y. Li, “Structural, electronic, and magnetic properties of a series of aluminum clusters doped with various transition metals,” Chemical Physics Letters, vol. 480, no. 4–6, pp. 258–264, 2009.

[48] D. Nematov, “Analysis of the optical properties and electronic structure of semiconductors of the Cu_2NiXS_4 (X = Si, Ge, Sn) family as new promising materials for optoelectronic devices,” arXiv preprint arXiv:2601.02434, 2026.

[49] D. Nematov, “Bandgap tuning and analysis of the electronic structure of the Cu_2NiXS_4 (X = Sn, Ge, Si) system: mBJ accuracy with DFT expense,” Chemistry of Inorganic Materials, vol. 1, p. 100001, 2023.

[50] E. Finazzi, C. Di Valentin, G. Pacchioni, and A. Selloni, “Excess electron states in reduced bulk anatase TiO_2: Comparison of standard GGA, GGA+U, and hybrid DFT calculations,” The Journal of Chemical Physics, vol. 129, no. 15, 2008.

[51] Y. Gao et al., “First-principles calculations of the electronic structure and optical properties of high-throughput doped SnO by the HSE06 method,” Applied Physics A, vol. 132, no. 1, p. 56, 2026.

[52] Z. Zhao and Q. Liu, “Effects of lanthanide doping on electronic structures and optical properties of anatase TiO_2 from density functional theory calculations,” Journal of Physics D: Applied Physics, vol. 41, no. 8, p. 085417, 2008.

[53] N. H. Hong, “Ferromagnetism in transition-metal-doped semiconducting oxide thin films,” Journal of Magnetism and Magnetic Materials, vol. 303, no. 2, pp. 338–343, 2006.

[54] Ahmed, T.Y., Saeed, S.R., Abdullah, O.G. and Aziz, S.B., 2026. Supercell design via first principle calculation approach to investigate the band structure and optoelectronic properties of α-Al_2O_3 doped with indium, boron, and arsenic. Physica Scripta, 101(18), p.185910.

[55] Benam, M.R., Rahnamaye Aliabad, H.A. and Hosseini, S.M., 2006. Effect of substituted IIIB transition metals on the energy gap of α-Al_2O_3 by first-principle calculations. physica status solidi (a), 203(9), pp.2223-2228.

[56] A Rahnamaye Aliabad, H., 2015. Investigation of optoelectronic properties of pure and Co substituted α- Al_2O_3 by Hubbard and modified Becke-Johnson exchange potentials. Chinese Physics B, 24(9), p.097102.

[57] Abd Halim, N.A.F., Razali, W.A.W., Yaakob, M.K., Ridzwan, M.H., Mohamed, Z., Matmin, J. and Hashim, A., 2023. The role of chromium on the structural, electronic and photoluminescence properties of alumina: theoretical and experimental study. Inorganic Chemistry Communications, 149, p.110437.

[58] A. V. Bandura, J. D. Kubicki, and J. O. Sofo, "Comparisons of multilayer H_2O adsorption onto the (110) surfaces of α-TiO_2 and SnO_2 as calculated with density functional theory," The Journal of Physical Chemistry B, vol. 112, no. 37, pp. 11616–11624, 2008.

[59] S. D. Mo and W. Y. Ching, "Electronic and optical properties of three phases of Al_2O_3: α, θ, and κ," Physical Review B, vol. 57, no. 24, pp. 15219–15228, 1998.

[60] K. Matsunaga, A. Nakamura, T. Yamamoto, and Y. Ikuhara, "First-principles study of defect energetics in titanium-doped alumina," Physical Review B, vol. 68, no. 21, p. 214102, 2003.

[61] Y. Ye, M. Kapilashrami, C. H. Chuang, Y. S. Liu, P. A. Glans, and J. Guo, "X-ray spectroscopies studies of the 3d transition metal oxides and applications of photocatalysis," MRS Communications, vol. 7, no. 1, pp. 53–66, 2017.

[62] I. Galanakis and P. Mavropoulos, "Spin-polarization and electronic properties of half-metallic Heusler alloys calculated from first principles," Journal of Physics: Condensed Matter, vol. 19, no. 31, p. 315213, 2007.

[63] Dash, S., Behera, D., Mohanty, S.K., Palai, G. and Mohanty, S., 2026. Pioneering computational insights into $KZrS_3$ and $KZrSe_3$ for future optoelectronics. *Phase Transitions*, pp.1-16.

[64] Swain, K., Kumari Mohanty, R., Palai, G., Dash, S. and Kalyan Mishra, B., 2026. Thermal effects on the emission characteristics of colloidal quantum dots for laser-driven color conversion applications. *Journal of Russian Laser Research*, pp.1-13.

[65] G. Mei-Li, Z. Xiao-Dong, L. Chun-Tian, and J. Guo-Zhi, "Mechanism of visible photoactivity of F-doped TiO_2," Chinese Physics Letters, vol. 27, no. 5, p. 057103, 2010.

[66] H. Chen, "Calculations of optical properties in anatase TiO_2," Chinese Journal of Luminescence, vol. 30, no. 5, pp. 697–701, 2009.

[67] R. A. Khalil et al., "Effect of dopants on the structural, optoelectronic and magnetic properties of pristine AgGaO3 perovskite: A first principles study," Optik, vol. 244, p. 167555, 2021.

[68] Y. Liu, Q. Hou, S. Sha, and Z. Xu, "Electronic structure, optical and ferromagnetic properties of ZnO co-doped with Ag and Co according to first-principles calculations," Vacuum, vol. 173, p. 109127, 2020.

[69] S. W. Fan, Z. H. Liu, Z. B. Li, and W. B. Li, "Electronic structure and magnetism for Cu-doped ZnO by GGA and GGA+mBJ density functional calculation," Journal of Henan Polytechnic University (Natural Science), vol. 32, no. 1, pp. 114–117, 2013.

[70] H. Chen, Y. Qu, L. Sun, J. Peng, and J. Ding, "Band structures and optical properties of Ag and Al co-doped ZnO by experimental and theoretic calculation," Physica E: Low-dimensional Systems and Nanostructures, vol. 114, p. 113602, 2019.

[71] Z. K. Heiba, M. B. Mohamed, and A. M. Wahba, "Structural, optical, mechanical, and electronic properties of Cr-doped alumina," Journal of Materials Science: Materials in Electronics, vol. 31, no. 17, pp. 14645–14657, 2020.

[72] D. M. Mamand et al., "Theoretical and experimental investigation on ADT organic semiconductor in different solvents," Condensed Matter and Interphases, vol. 24, no. 2, pp. 227–242, 2022.

[73] T. V. Vu et al., “Electronic and optical properties of wide band gap Tl3TaS4: A promising surface acoustic wave material,” Optical Materials, vol. 99, p. 109601, 2020.

[74] T. Y. Ahmed, S. R. Saeed, S. B. Aziz, and O. G. Abdullah, “Enhancing electronic and optical properties of NiO using Cu-doping: A DFT approach for band gap reduction,” Oxford Open Materials Science, vol. 5, no. 1, p. itaf009, 2025.

[75] K. K. Ahmed et al., “A brief review on optical properties of polymer composites: insights into light-matter interaction from classical to quantum transport point of view,” Results in Physics, vol. 56, p. 107239, 2024.